Key role for IL-21 in experimental autoimmune uveitis

Lu Wang[a,1], Cheng-Rong Yu[b,1], Hyoung-Pyo Kim[a,c,1], Wei Liao[a], William G. Telford[d], Charles E. Egwuagu[b,2], and Warren J. Leonard[a,2]

[a]Laboratory of Molecular Immunology, National Heart, Lung, and Blood Institute, Bethesda, MD 20892; [b]Laboratory of Immunology, National Eye Institute, Bethesda, MD 20892; [c]Department of Environmental Medical Biology, Institute of Tropical Medicine and Brain Korea 21 Project for Medical Science, Yonsei University College of Medicine, Seoul 120-752, Korea; and [d]Experimental Transplantation and Immunology Branch, National Cancer Institute, National Institutes of Health, Bethesda, MD 20892

Edited* by Rafi Ahmed, Emory University, Atlanta, GA, and approved April 25, 2011 (received for review December 7, 2010)

IL-21 is a pleiotropic type 1 cytokine that shares the common cytokine receptor γ-chain, γ_c, with IL-2, IL-4, IL-7, IL-9, and IL-15. IL-21 is most homologous to IL-2. These cytokines are encoded by adjacent genes, but they are functionally distinct. Whereas IL-2 promotes development of regulatory T cells and confers protection from autoimmune disease, IL-21 promotes differentiation of Th17 cells and is implicated in several autoimmune diseases, including type 1 diabetes and systemic lupus erythematosus. However, the roles of IL-21 and IL-2 in CNS autoimmune diseases such as multiple sclerosis and uveitis have been controversial. Here, we generated *Il21*-mCherry/*Il2*-emGFP dual-reporter transgenic mice and showed that development of experimental autoimmune uveitis (EAU) correlated with the presence of T cells coexpressing IL-21 and IL-2 into the retina. Furthermore, *Il21r*$^{-/-}$ mice were more resistant to EAU development than wild-type mice, and adoptive transfer of *Il21r*$^{-/-}$ T cells induced much less severe EAU, underscoring the need for IL-21 in the development of this disease and suggesting that blocking IL-21/γ_c–signaling pathways may provide a means for controlling CNS auto-inflammatory diseases.

IL-21 is a type 1 four-α-helical-bundle cytokine with major actions on a range of lymphoid populations (1). IL-21 signals via IL-21R and the common cytokine receptor γ-chain, γ_c (1), which is mutated in humans with X-linked severe combined immunodeficiency (2) and is shared by the receptors for IL-2, IL-4, IL-7, IL-9, IL-15, and IL-21 (3). IL-21 is produced mainly by $CD4^+$ T cells, including Th17 cells (1, 4), T follicular helper cells (5), and natural killer (NK) T cells (6). It promotes the function and expansion of effector $CD8^+$ T cells (7) and can activate NK cells (8). It is also critical for B-cell differentiation into plasma cells and Ig production (9, 10) and negatively regulates the function of dendritic cells (11). IL-21 plays a role in autoimmune diseases, including type I diabetes in nonobese diabetic mice (12, 13), systemic lupus erythematosus in MRL/*lpr* and BXSB/*Yaa* mice (9, 14, 15), and collagen-induced arthritis (16). In experimental allergic encephalitis (EAE), divergent effects of IL-21 have been reported related to its role in the development and progression of the autoimmune response as well as whether it is required for disease development (1, 17, 18).

The genes encoding IL-21 and IL-2 are adjacent and share similar genomic organization in humans and mice (19). Coevolution of the IL-21 and IL-2 systems is further suggested not only by their sharing of γ_c but also by the fact that IL-21R is most closely related to IL-2Rβ (20); nevertheless, IL-21 and IL-2 have distinct functions. For example, IL-21 is implicated in the development of autoimmunity (9, 12–14, 16), but mice deficient in IL-2, IL-2Rα, and IL-2Rβ exhibit autoimmunity (21–24), suggesting that IL-2 protects against development of autoimmune disease. IL-21 can promote the development of Th17 cells, whereas IL-2 inhibits the differentiation of Th17 cells (25), although it induces the expansion of Th17 cells that mediate uveitis and scleritis (26).

Uveitis is a group of sight-threatening idiopathic intraocular inflammatory diseases including Behçet's disease, birdshot retinochoroidopathy, sympathetic ophthalmia, Vogt-Koyanagi-Harada, and ocular sarcoidosis, which may be of infectious or autoimmune etiology (27). Experimental autoimmune uveitis (EAU) shares pathological features with human uveitis, and much of our understanding of the etiology and pathophysiology of this disease derives from studies of EAU (27, 28). EAU can be induced in susceptible rodent species by immunization with the retinal protein, interphotoreceptor retinoid-binding protein (IRBP) (*Materials and Methods*). Although the etiology of noninfectious uveitis is unknown, patients with uveitis have more IL-17–producing T cells (Th17) in peripheral blood than healthy individuals (29). Moreover, Th17 cells increase during active uveitis but decrease after treatment, suggesting that they play a role in the disease process (26). Consistent with a role for Th17 cells in CNS autoimmune diseases, mice with targeted deletion of the *Stat3* gene in T cells cannot generate Th17 cells and do not develop EAU or EAE (30), indicating the importance of Th17 cells in uveitis and multiple sclerosis. Because IL-21 is produced by Th17 cells, mediates its biological actions in part via STAT3, and promotes Th17 differentiation, IL-21 could be a potential mediator of EAU.

An impediment to the study of the role of IL-21–expressing T cells in disease has been the absence of high-quality Abs for detecting in situ expression of IL-21 in tissues by intracellular staining. In this study, we generated bacterial artificial chromosome (BAC) reporter transgenic (Tg) mice in which the promoters of the adjacent *Il2* and *Il21* genes in a BAC clone spanning both genes direct expression of emGFP and mCherry, respectively. These mice allowed us to investigate in vivo the presence of IL-21 (mCherry) and/or IL-2 (emGFP)–expressing T cells in lymph nodes (LNs) and to monitor their infiltration into the retina during EAU. We detected a substantial increase in T cells expressing *Il2*-emGFP and *Il21*-mCherry in LNs before the onset of inflammation, and these cells were subsequently detected in the retina of mice with EAU, suggesting their involvement in the pathogenic mechanism of uveitis. We also found that *Il21r*$^{-/-}$ mice have defective development of EAU, and involvement of IL-21 in this disease was further shown by adoptive transfer experiments.

Results

Identification of IL-21– and IL-2–Expressing Cells in Vivo Using *Il21*-mCherry/*Il2*-emGFP Reporter Mice. To evaluate IL-21 and IL-2 gene expression, we generated *Il21*-mCherry and *Il2*-emGFP BAC dual reporter Tg mice (Fig. 1*A*). For most experiments, we used a

Author contributions: L.W., C.-R.Y., H.-P.K., W.L., W.G.T., C.E.E., and W.J.L. designed research; L.W., C.-R.Y., H.-P.K., and W.L. performed research; L.W., C.-R.Y., H.-P.K., W.G.T., C.E.E., and W.J.L. analyzed data; and L.W., C.-R.Y., H.-P.K., W.G.T., C.E.E., and W.J.L. wrote the paper.

Conflict of interest statement: W.J.L. is an inventor on patents and patent applications related to IL-21.

*This Direct Submission article had a prearranged editor.

[1]L.W., C.-R.Y., and H.-P.K. contributed equally to this work.

[2]To whom correspondence may be addressed. E-mail: wjl@helix.nih.gov or egwuaguc@nei.nih.gov.

This article contains supporting information online at www.pnas.org/lookup/suppl/doi:10.1073/pnas.1018182108/-/DCSupplemental.

founder line containing one integrated copy of the reporter construct, but behavior of a second independent BAC reporter mouse line was similar (Fig. S1 *A* and *B*). To validate the reporter mice, we stimulated $CD4^+$ T cells enriched from the Tg reporter and wild-type (WT) littermate mice with anti-CD3 and anti-CD28 and analyzed the expression of emGFP and IL-2 by flow cytometry (Fig. 1*B*). The frequency of IL-2^+ cells determined by intracellular staining was ∼35% in both Tg reporter mice and WT controls. In the reporter mice, >95% of $emGFP^+$ cells also produced IL-2, and ∼70% of IL-2–producing cells were $emGFP^+$, even though our fixation procedure included paraformaldehyde, which can quench the emGFP fluorecence. We also stimulated $CD4^+$ T cells with anti-CD3 + anti-CD28 and sorted $emGFP^-$ and $emGFP^+$ cells. By intracellular staining, 60% of the $emGFP^+$ but only 11% of $emGFP^-$ cells were IL-2^+ (Fig. S2*A*). Moreover, we evaluated IL-2 and IL-21 mRNA expression of sorted $emGFP^-mCherry^-$ double-negative (DN), $emGFP^+$ and $mCherry^+$ single-positive, and $emGFP^+mCherry^+$ double-positive (DP) cells by real-time PCR. $mCherry^+$ and DP cells had ∼30-fold higher IL-21 mRNA expression than DN cells. As expected, IL-21 mRNA expression in GFP^+ cells was weaker. $emGFP^+$ cells had higher IL-2 mRNA expression than DN and $mCherry^+$ cells, and IL-2 mRNA expression of DP cells was less than in GFP^+ cells but still fivefold higher than in DN cells (Fig. 1*C*). We also stimulated $CD4^+$ T cells with anti-CD3 + anti-CD28 with or without IL-6 and TGF-β for 18 h and evaluated mRNA expression of mCherry, IL-21, emGFP, and IL-2 by RT-PCR. Levels of mCherry and IL-21 mRNA were highly correlated ($R^2 = 0.99$) as were emGFP and IL-2 mRNA ($R^2 = 0.89$) (Fig. 1*D*), further validating the *Il2*-emGFP/*Il21*-mCherry reporter mice.

We next stimulated $CD4^+$ T cells with anti-CD3 + anti-CD28 under neutral conditions (presence of anti–IFN-γ + anti–IL-4) versus Th1 or Th17 conditions and analyzed cells at days 1, 2, and 3 (Fig. 1*E*). emGFP as a marker for IL-2 increased under all conditions but least under Th17 conditions, whereas mCherry as a marker of IL-21 production was highest in Th17 cells. As expected, Th1 cells expressed both emGFP and mCherry, consistent with their known production of IL-21 (1) as well as of IL-2. Sorting of cells after Th1 stimulation revealed that ∼28.5% of $emGFP^+$ cells produced IFN-γ versus <2% of $mGFP^-$ cells (Fig. S2*B*). Similarly, sorting of cells after Th17 differentiation revealed that ∼11% of the $mCherry^+$ cells produced IL-17A versus <3% of $mCherry^-$ cells (Fig. S2*C*).

To identify IL-21– and IL-2–producing cells in vivo, we next examined *Il21*-mCherry/*Il2*-emGFP expression in liver, spleen, and other lymphoid tissues. $CD4^+$ cells that expressed mCherry, emGFP, or both were present in all tissues examined, but the frequencies of the cell subsets differed in different tissues (Fig. 1*F*). Approximately 1–2% of $CD4^+$ T cells in spleen, as well as axillary, cervical, and mesenteric LNs, were *Il2*-$emGFP^+$, in contrast to ∼0.5% in the liver, whereas there were more of these

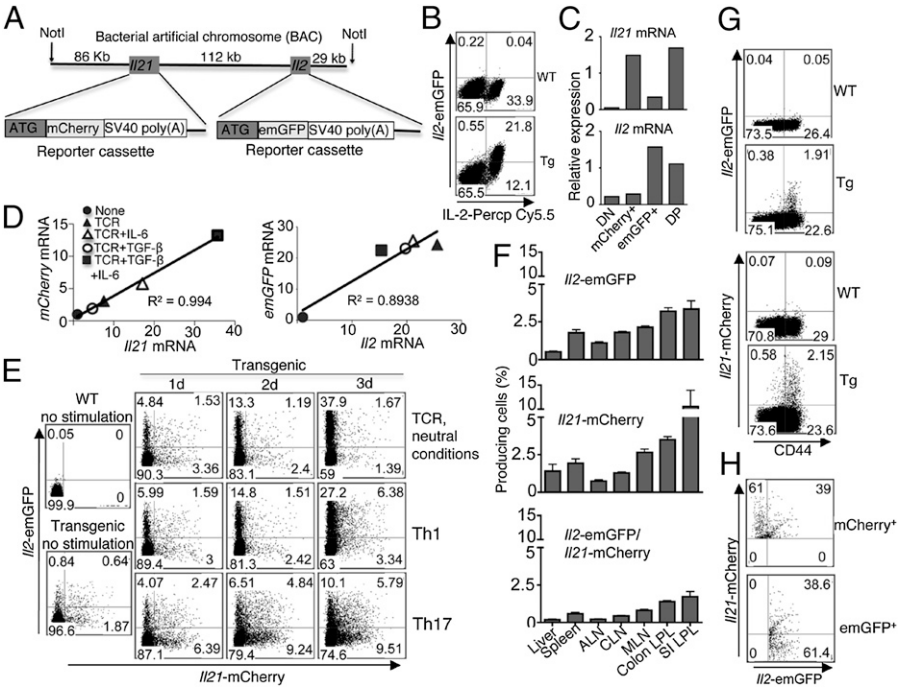

Fig. 1. Characterization of *Il21*-mCherry/*Il2*-emGFP reporter Tg mice. (*A*) Shown is a BAC containing the *Il21* and *Il2* genes, with mCherry and emGFP introduced. (*B*) Splenic $CD4^+$ T cells from control and reporter Tg mice were stimulated with anti-CD3 + anti-CD28 for 3 d, restimulated with PMA and ionomycin for 4 h, and then surface-stained for CD4 and intracellularly stained for IL-2. The plots were gated on $CD4^+$ cells. Shown is one of four experiments with similar results. (*C*) $mCherry^-emGFP^-$ DN, single-positive ($mCherry^+$), emGFP single-positive ($emGFP^+$), and $mCherry^+emGFP^+$ DP were sorted from $CD4^+$ T cells from the reporter Tg mice. IL-21 and IL-2 mRNAs were measured by real-time PCR. Data are from LNs pooled from 14 mice. (*D*) $CD4^+$ T cells from reporter Tg mice were not stimulated or were stimulated with anti-CD3 + anti-CD28, without or with IL-6, TGF-β, or both IL-6 and TGF-β for 18 h. IL-21, mCherry, IL-2, and emGFP mRNAs were measured by RT-PCR. Correlation of IL-21 versus mCherry mRNA and of IL-2 versus emGFP mRNA expression are shown by R^2 values. Shown is one of two experiments with similar results. (*E*) $CD4^+$ T cells from reporter Tg mice were polarized as indicated for 3 d. Shown are *Il2*-emGFP and *Il21*-mCherry expression at days 1, 2, and 3. Shown is one of three experiments with similar results. (*F*) *Il2*-emGFP and *Il21*-mCherry expression in $CD4^+$ T cells isolated from reporter Tg mice or WT littermate controls. The bar graphs indicate data from gating on $CD4^+$ T cells. ALN, axillary lymphocytes; CLN, cervical lymphocytes; MLN, mesenteric lymphocytes; SI LPL, small intestine lamina propria lymphocytes. Shown is mean ± SD for three independent experiments. (*G*) Splenocytes from reporter Tg mice were analyzed by flow cytometry for expression of CD4, CD44, emGFP, and mCherry, gated on $CD4^+$ T cells. Shown is one of three experiments with similar results. (*H*) Expression of mCherry and emGFP is shown. (*Upper*) Gated on $CD4^+CD44^{high}mCherry^+$ cells. (*Lower*) Gated on $CD4^+CD44^{high}emGFP^+$ cells. Shown is one of three experiments with similar results.

cells (3–4% of $CD4^+$ T cells) in the small intestine lamina propria lymphocytes (SI LPLs) and in the colon LPLs, consistent with higher basal stimulation in the gut (Fig. 1*F*, *Top*). For *Il21*-mCherry, expression tended to be lowest in liver, axillary, and cervical LNs, slightly higher in spleen, mesenteric LNs, and colon, and highest (10% of cells) in SI LPLs (*Middle*). Cells expressing both *Il2*-emGFP$^+$ and *Il21*-mCherry were detected in all tissues, but were highest in the gut (*Bottom*). Thus, *Il2*-emGFP$^+$ and *Il21*-mCherry$^+$ cells were present in all immune compartments examined, with relative enrichment in the intestine. Evaluation of splenic $CD4^+$ T cells revealed that ~80% of these *Il2*-emGFP$^+$ and *Il21*-mCherry$^+$ cells were $CD44^{hi}CD4^+$ effector/memory type T cells (Fig. 1*G*). When we gated on $CD4^+CD44^+$mCherry$^+$ and $CD4^+CD44^+$emGFP$^+$ cells, 39% of *Il21*-mCherry$^+$ cells and 38.6% of *Il2*-emGFP$^+$ cells were both mCherry$^+$ and emGFP$^+$ (Fig. 1*H*).

Augmented Expression of IL-21 and IL-2 Expression in EAU. We next immunized the reporter Tg mice with IRBP and examined mCherry and emGFP expression at day 21, at which point mice had developed severe uveitis. After immunization, we detected *Il2*-emGFP$^+$ $CD4^+$ T cells in draining LNs (Fig. 2 *A* and *Left Panel* of *B*). mCherry also increased from 2% of $CD4^+$ T cells before immunization to ~9% afterward (Fig. 2*B*, *Center*). After immunization, ~4% of $CD4^+$ cells were *Il21*-mCherry$^+$/*Il2*-emGFP$^+$ DP cells (Fig. 2*B*, *Right*). From 50,000 LN cells for each sample, mCherry$^+$ cells increased from ~220 to ~590 cells after immunization. emGFP$^+$ cells and DP cells increased from ~200 to ~500 and from ~90 to ~210 cells, respectively (Fig. 2*C*). Similar results were obtained with a second reporter BAC Tg mouse line containing six copies of the BAC clone rather than one (Fig. S1). We also sorted DN, emGFP$^+$, mCherry$^+$, and DP cells from $CD4^+$-draining lymphocytes 21 d after immunization

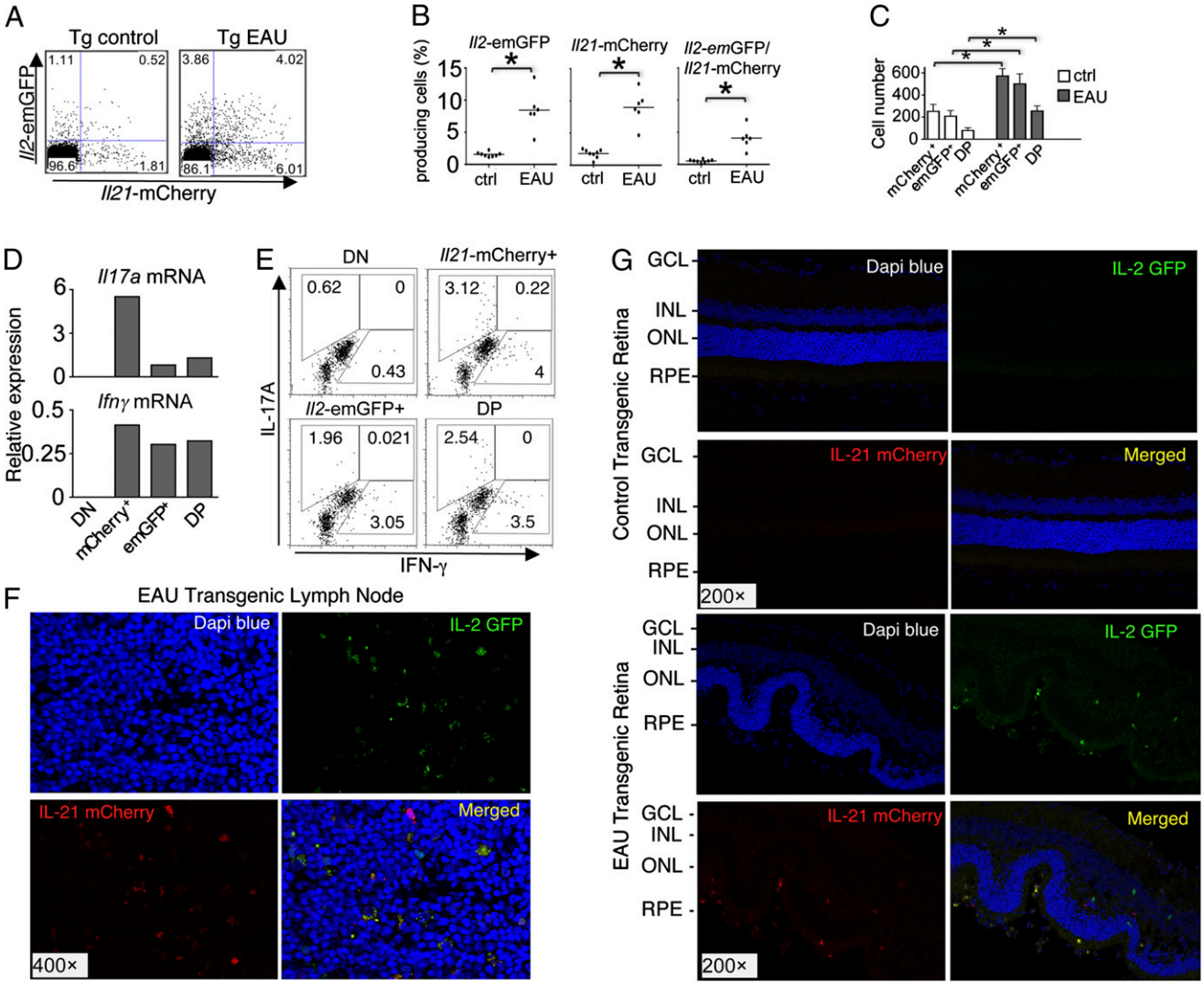

Fig. 2. Increased *Il2*-emGFP and *Il21*-mCherry expression after EAU induction (*A* and *B*) Expression of *Il2*-emGFP and *Il21*-mCherry in draining lymphocytes from reporter Tg mice 21 d after immunization with IRBP, gated on $CD4^+$ cells. Shown are representative mice from one of two experiments with similar results ($n = 8$ for Tg control and $n = 6$ for Tg EAU). (*B*) Summary of flow cytometric profiles of $CD4^+$ T cells from eight Tg control and six Tg EAU mice from the experiment in *A*. Shown are *Il2*-emGFP$^+$, *Il21*-mCherry$^+$, and *Il21*-mCherry$^+$*Il2*-emGFP$^+$ DP cells. *$P < 0.05$. (*C*) From the experiment in *A*, 50,000 cells for each Tg control and Tg EAU were analyzed. Shown are the number of mCherry$^+$, emGFP$^+$, and *Il21*-mCherry$^+$*Il2*-emGFP$^+$ DP cells. *$P < 0.05$. (*D* and *E*) mCherry$^-$ and emGFP$^-$ DN, mCherry$^+$, emGFP$^+$, and mCherry$^+$emGFP$^+$ DP cells were sorted from $CD4^+$ T cells from pooled LNs from reporter Tg mice 21 d after immunization with IRBP. In *D*, IL-17A and IFN-γ mRNAs were measured by real-time PCR. In *E*, cells were stimulated with PMA + ionomycin for 4 h, and IL-17A and IFN-γ were measured by intracellular staining. (*F*) Frozen sections of LNs from reporter Tg mice 7 d after immunization were stained with DAPI. Red, mCherry; green, emGFP. (*G*) Frozen sections of eyes from unimmunized and immunized reporter Tg mice at day 21. GCL, ganglion cell layer; INL, inner nuclear layer; ONL, outer nuclear layer, RPE, retinal pigment epithelial layer. Shown is one of seven experiments with similar results.

and performed both RT-PCR and intracellular staining. As expected, mCherry$^+$ cells had high *Il17a* mRNA expression (Fig. 2*D*), consistent with IL-17A cytokine production (Fig. 2*E*). *Ifng* mRNA was expressed in emGFP$^+$, mCherry$^+$, and DP cells (Fig. 2*D*), and correspondingly, IFN-γ protein was produced by these three populations (Fig. 2*E*). We also examined IL-21– and IL-2–producing cells in draining LNs and retina using confocal microscopy and reporter Tg mice not immunized or immunized with IRBP. *Il21*-mCherry and *Il2*-emGFP were expressed in draining LNs at day 7 (Fig. 2*F*) and in the eye at day 21 after immunization (Fig. 2*G*). Of the emGFP$^+$ and/or mCherry$^+$ cells infiltrating the retina, ~50% were *Il2*-emGFP$^+$, ~25% were *Il21*-mCherry$^+$, and ~25% were DP cells (Fig. S3). Thus, during EAU development, expression of both IL-2 and IL-21 was induced in autoreactive CD4$^+$ T cells, and cells expressing each cytokine as well as cells expressing both cytokines were present in the inflammatory cells infiltrating the retina.

Less Severe EAU in *Il21r*$^{-/-}$ Mice. Given the role of IL-21 in the development of autoimmune diseases and its expression within the retina, we investigated the development of EAU in WT versus *Il21r*$^{-/-}$ mice, monitoring by fundoscopy from day 10 after immunization to the end of the study period (approximately day 25). Compared with the normal control (Fig. 3*A*, *Left*), WT retinas at day 21 showed severe inflammation with blurring of the optic disk margins, retinal vasculitis with cuffing (red asterisks), and inflammatory infiltrates (black arrows) (Fig. 3*A*, *Center*). Histological analysis revealed massive inflammatory cell infiltration in the vitreous (black arrows), photoreceptor cell damage and retinal folds (Fig. 3*B*, blue arrows), and choroiditis (Fig. 3*B*, *Center* panels). In contrast, *Il21r*$^{-/-}$ mice had modest fundoscopic changes, with less inflammation, only slight retinal vasculitis with cuffing (red asterisk) (Fig. 3*A*, *Right*), and less severe histological changes (Fig. 3*B*, *Right* panels). EAU scores based on fundoscopy (31) (Fig. 3*C*) or histology (32) (Fig. 3*D*) showed much less disease in the *Il21r*$^{-/-}$ mice. Correspondingly, at day 21, the proliferation of draining LN cells from EAU WT mice was greater than in unimmunized animals in response to IRBP (Fig. 3*E*). Proliferation was induced by immunization with IRBP in *Il21r*$^{-/-}$ mice but was lower than in WT mice (Fig. 3*E*). IL-17–expressing and IFN-γ–expressing T cells have been implicated in EAU (26). We therefore examined the production of IL-2, IL-17, and IFN-γ from CD4$^+$ T cells in peripheral blood mononuclear cells (PBMCs) after EAU induction. There was significantly less

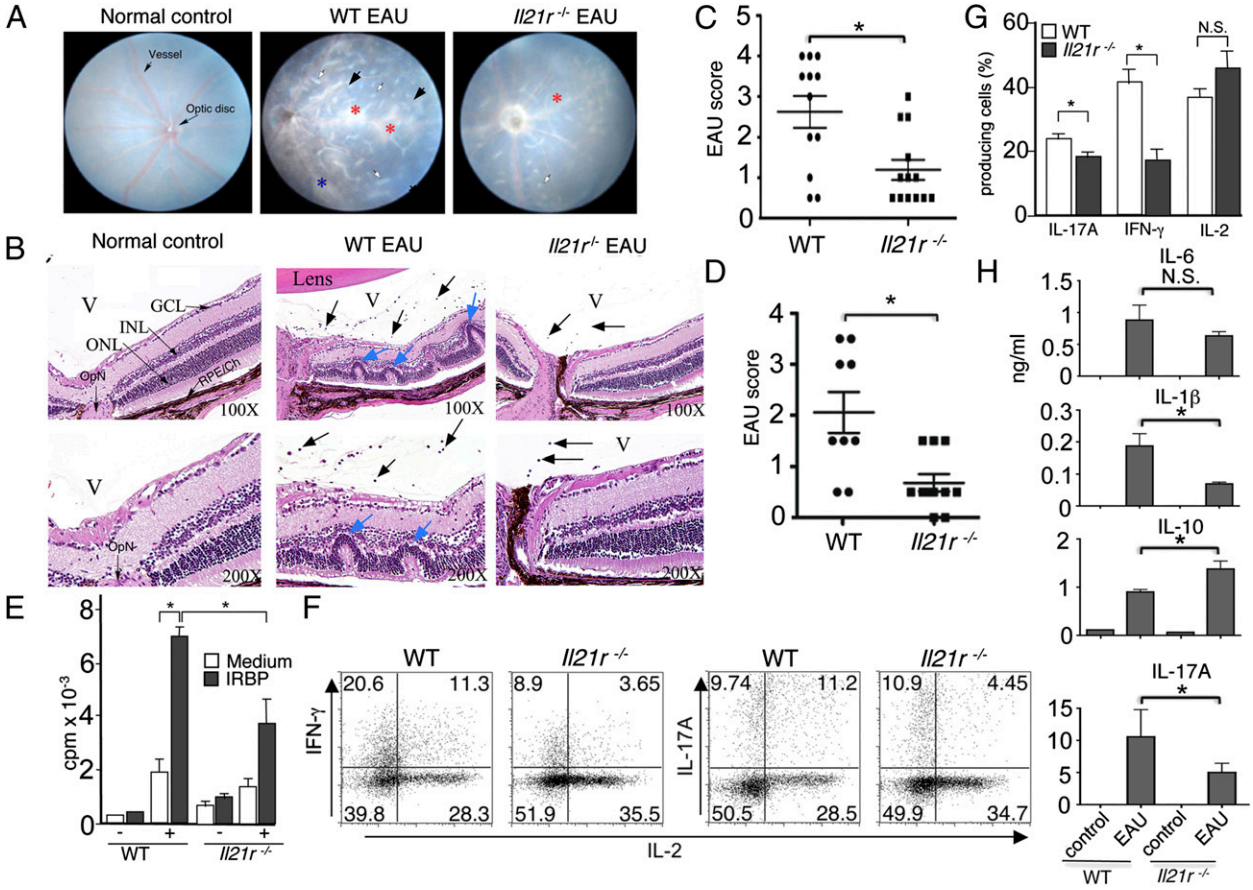

Fig. 3. Loss of IL-21 signaling protects mice from EAU. (*A*) Fundus images from C57BL/6 WT mouse (*Left*) and WT or *Il21r*$^{-/-}$ mice 20 d postimmunization with IRBP (*Center* and *Right*). Red asterisks, retinal vasculitis with cuffing; black arrows, inflammatory infiltrates; blue asterisk, severe retinal infiltrates, choroiditis, and vasculitis with cuffing. (*B*) Histological sections of eyes from WT and *Il21r*$^{-/-}$ mice 21 d post-IRBP. OpN, optic nerve; INL, inner nuclear layer; ONL, outer nuclear layer; black arrows, inflammatory cells in vitreous; blue arrows, retinal fold. Shown is 1 of 10 mice with similar results. (*C* and *D*) EAU score of C57BL/6 WT and *Il21r*$^{-/-}$ mice based on fundoscopy (*C*) and histology (*D*). Shown is mean ± SEM of 10 mice in each group. *$P < 0.05$ ($P = 0.0105$). (*E*) LN cells from WT and *Il21r*$^{-/-}$ control and EAU mice were cultured without or with IRBP in complete medium for 2 d and pulsed with [^{3}H]thymidine for 12 additional hr. Shown are mean ± SEM from five replicate cultures. *$P < 0.01$. (*F* and *G*) PBMCs from WT and *Il21r*$^{-/-}$ mice were isolated 21 d after immunization and stimulated with PMA + ionomycin for 4 h. Intracellular staining of IL-17A, IFN-γ, and IL-2 in CD4$^+$ T cells was performed. (*F*) Data from one of three experiments with pooled cells from three to four mice each. (*G*) Summary of the data from all three experiments (mean ± SD). (*H*) Cells from draining LNs at day 21 from IRBP-immunized WT and *Il21r*$^{-/-}$ mice were stimulated with IRBP peptide for 3 d. IL-6, IL-1β, IL-10, and IL-17 levels in culture supernatant was measured by ELISA. Data represent mean ± SD ($n = 5$ for IL-6, IL-1β, and IL-10 and $n = 7$ for IL-17A). N.S., $P > 0.05$ ($P = 0.09$). *$P < 0.05$.

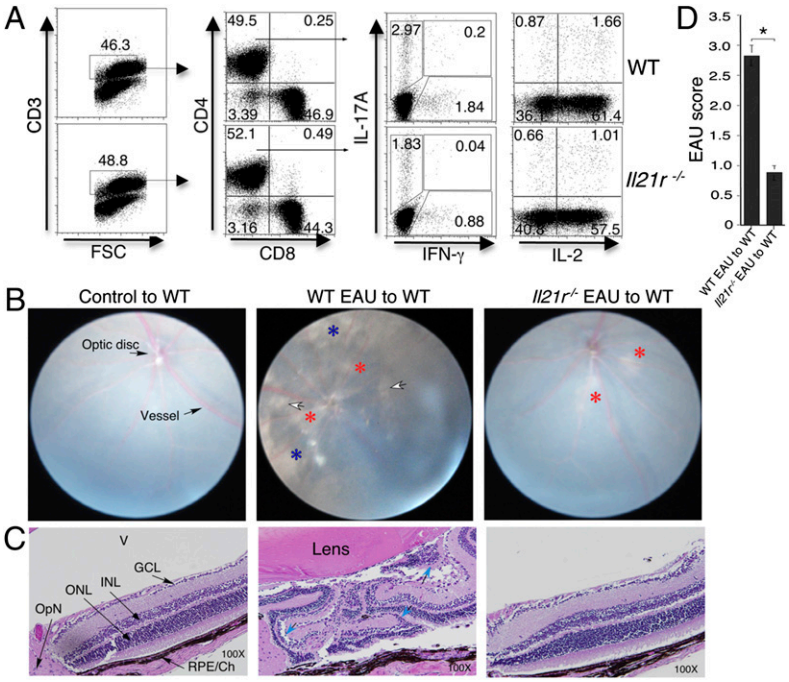

Fig. 4. *Il21r*$^{-/-}$ mice are defective in generating IRBP-specific pathogenic T cells. Draining LN cells from WT and *Il21r*$^{-/-}$ EAU mice were stimulated with IRBP for 4 d and then adoptively transferred into C57BL/6 WT mice. (*A*) WT and *Il21r*$^{-/-}$ EAU mice were stimulated in vitro before adoptive transfer. Percentage of CD3$^+$ and CD4$^+$ T cells are shown in the first two panels. We gated on CD4$^+$ T cells and measured the percentage of IL-17A–, IFN-γ–, and IL-2–producing cells (last two panels). (*B*) Fundoscopy was performed 14 d later. White arrows, inflammatory infiltrates; red asterisks, retinal vasculitis with cuffing; blue asterisks, severe retinal infiltrates and scars and choroiditis. (*C*) Histological sections of eyes of EAU-adoptively transferred C57BL/6 WT mice, as indicated. Blue arrows, retinal fold. (*D*) Shown is the EAU clinical score of adoptive transfer EAU based on fundoscopy images by the Mann–Whitney test. Shown is mean ± SEM. *$P < 0.01$. $n = 4$ mice in each group.

IL-17 and IFN-γ production in *Il21r*$^{-/-}$ mice, but IL-2 production was similar in WT and *Il21r*$^{-/-}$ mice (Fig. 3 *F* and *G*). Moreover, when draining LN cells were harvested at day 21 and then stimulated with IRBP for 3 d, there was less IL-17A and IL-1β but more IL-10 production in *Il21r*$^{-/-}$ mice (Fig. 3*H*). IL-6 production tended to be lower, but the difference was not significant (Fig. 3*H*). Overall, these data indicate a possible shift from pro- to anti-inflammatory cytokines in the absence of IL-21 signaling.

Adoptive Transfer of IRBP-Specific Uveitogenic Lymphocytes from *Il21r*$^{-/-}$ Mice Induces Less Severe EAU than WT Cells. To confirm that the *Il21r*$^{-/-}$ mouse defect occurred in the generation of IRBP-specific pathogenic T cells, we adoptively transferred WT and *Il21r*$^{-/-}$ IRBP-specific lymphocytes into WT mice. We found similar CD3 and CD4/CD8 profiles (Fig. 4*A*, *Left* and *Center* panels), but the *Il21r*$^{-/-}$ cells produced less IL-17A and IFN-γ but similar levels of IL-2 (Fig. 4*A*). Compared with mice receiving WT cells, animals receiving *Il21r*$^{-/-}$ cells exhibited less severe EAU as evaluated by fundoscopy (Fig. 4*B*), histological analysis (Fig. 4*C*), and clinical EAU score (Fig. 4*D*).

Discussion

In this study, we investigated the role of IL-21 in EAU development. The expression of IL-21 in draining LNs and retina, as revealed by the *Il21*-mCherry/*Il2*-emGFP reporter mice; the diminished development of EAU in *I l21r*$^{-/-}$ mice; and the less severe EAU following adoptive transfer of IRBP-specific lymphocytes from *Il21r*$^{-/-}$ mice together underscore the importance of IL-21 in the development of EAU. WT mice mounted a higher IL-17 response than did *Il21r*$^{-/-}$ mice. Given that IL-21 can promote Th17 cell differentiation (1), it is possible that the lack of IL-21 signaling protects mice from EAU through a mechanism involving decreased production of IL-17, which has been suggested to be important for the development of both EAU (26, 29) and EAE (17). Previously, IL-21 was shown to play important roles in animal models of type 1 diabetes (12, 13) and systemic lupus erythematosus (14, 15). Our data now implicate this cytokine in a model of autoimmunity causing disease at an immunologically "privileged" site as well, revealing its very broad contribution to autoimmunity.

By analyzing the location of *Il21*-mCherry$^+$ and *Il2*-emGFP$^+$ cells after inducing EAU, we infer that immunization by IRBP caused an immune response that produced both IL-21 and IL-2 in draining LNs, and both IL-21– and IL-2–producing cells were located in the eye at day 21, when severe inflammation is evident. Previously, IL-2 was reported to enhance protection from EAU in part by stimulating production of anti-inflammatory cytokines by regulatory T cells (33). The ability of IL-2 to inhibit Th17 differentiation (25) is another mechanism by which IL-2 might inhibit EAU. The fact that there were both IL-2– and IL-21–expressing cells in the inflammatory neuroretina in EAU is interesting, as both overlapping and distinctive actions for these cytokines have been noted (1, 34). Interestingly, IL-2 can expand Th17 cells once developed, potentially promoting uveitis and scleritis (26), and Daclizumab, a monoclonal antibody to IL-2Rα, can control inflammation in patients with noninfectious uveitis (35, 36), suggesting a role for IL-2 in the pathogenesis of this disease. Our data showing the presence of IL-2/IL-21 double-producer T cells in EAU extend these data.

In summary, we have shown a key role of IL-21 in the development of EAU, suggesting that interfering with the action of this cytokine may have therapeutic potential for uveitis. Moreover, we have generated *Il21*-mCherry/*Il2*-emGFP double reporter Tg mice to help study the role of IL-2 and IL-21 in the pathogenesis of EAU. These mice may be valuable for studying the potential roles for IL-2 and IL-21 in a broad range of other disease models as well.

Materials and Methods

Mice. *Il21r*$^{-/-}$ mice (10) were produced by breeding heterozygous mice. C57BL/6 mice were from the Jackson Laboratory. To generate *Il2*-emGFP/*Il21*-mCherry Tg reporter mice, we used the RP23-98I15 BAC clone (Invitrogen), which contains the *Il21* and *Il2* genes (Fig. 1*A*). Recombineering (37) was used to introduce the emGFP (Invitrogen) and mCherry (38) coding sequences linked to the SV40 poly(A) site into the first exon of the *Il2* and *Il21* genes, respectively. Recombineering comprises a two-step method to create precise genetic changes: first, *amp-sacB* is placed in the DNA and then this is replaced with the emGFP or mCherry coding sequences in a second recombineering event. The targeting cassettes with *amp-sacB* were amplified using primers with ≥50 bp 5′ overhangs that were homologous to the regions of the BAC just outside of the segment being replaced. The primers

are provided in *SI Materials and Methods*. BAC clones that had integrated the targeting construct were selected, and the location of the insert was confirmed by PCR and sequencing. The BAC was prepped using a Large-Construct kit (Qiagen), digested with NotI, DNA purified by phenol/chloroform extraction, and microinjected into fertilized C57BL/6J × CBA/J oocytes. Resulting pups were screened for the emGFP and mCherry reporters by PCR (see *SI Materials and Methods* for the primers). Founder lines were backcrossed at least six generations to C57BL/6 mice. Experiments were performed under protocols approved by the National Eye Institute and/or National Heart, Lung, and Blood Institute Animal Care and Use Committees.

Analysis of CD4$^+$ T-Helper Cells. For Th1 conditions, CD4$^+$ T cells (>98% pure) were treated with plate-bound 2 μg/mL anti-CD3 + soluble 1 μg/mL anti-CD28, 10 μg/mL anti–IL-4, and 10 ng/mL IL-12 for 3 d. For Th17 conditions, cells were treated with anti-CD3/CD28, 20 ng/mL IL-6, 2 ng/mL TGF-β1, and 10 μg/mL each of anti–IFN-γ and anti–IL-4. Cytokines and antibodies were from R & D Systems. For intracellular cytokine detection, cells were stimulated for 4 h with 10 ng/mL phorbol 2-myristate 3-acetate (PMA) + 1 μM ionomycin, Golgi-stop added in the last 2 h, and intracellular cytokine staining performed using a Cytofix/Cytoperm kit (BD Pharmingen). Flow cytometry was performed using a FACS-Calibur (BD Biosciences). All mAbs were from BD PharMingen. Flow cytometry was performed on an LSRII (BD Biosciences). mCherry was detected using a 561-nm laser with a 605/40 filter.

Real-Time PCR. mRNA was isolated from 10^6 cells (RNeasy mini kit; Qiagen) and cDNA was prepared (Omniscript RT kit, Qiagen). Real-time PCR was performed with an ABI PRISM 7700 sequence detection system with site-specific primers and probes (Applied Biosystems).

Induction and Evaluation of EAU. Mice were immunized with 150 μg bovine IRBP and 300 μg human IRBP peptide (amino acids 1–20) in 0.2 mL 1:1 vol/vol emulsion with complete Freund's adjuvant (CFA) containing *Mycobacterium tuberculosis* strain H37RA (2.5 mg/mL). Mice simultaneously received 0.3 μg *Bordetella pertussis* toxin. Clinical disease was scored by fundoscopy (31) and histological analysis (32), as detailed in *SI Materials and Methods*. Tissue sections were also examined using a multiphoton laser-scanning confocal microscope with fluorescence emission detected with 515/30 (emerald-GFP, green) and 600/40 (mCherry, red), as described (26, 31). For adoptive transfer experiments, draining LN cells from WT and *Il21r*$^{-/-}$ EAU mice (at day 21) were stimulated with IRBP 20 μg/mL for 4 d, and 10^7 cells in 200 μL of PBS were injected i.v. into sex- and age-matched recipient mice. Fundoscopic examinations were performed 14 d after adoptive transfer.

Cytokine Analysis and Lymphocyte Proliferation Assays. A total of 5×10^6 draining LN cells were cultured for 3 d in medium containing 10 μg/mL IRBP protein, and IL-6, IL-10, IL-1β, and IL-17 levels were measured using an ELISA kit (BD PharMingen). For proliferation, normal control and EAU draining lymphocytes (2×10^6/mL) were stimulated with 20 μg/mL IRBP. After 48 h, cultures were pulsed with [^{3}H]thymidine (0.5 μCi/10 μl/well) and incorporation was measured 12 h later.

Statistical Analyses. Nonparametric *t* tests and Prism software (Graphpad Software) were used.

ACKNOWLEDGMENTS. We thank Dr. Robert Fariss and Mercedes Campos for help with confocal microscopy, Barbara J. Taylor for help with FACS analysis, Dr. Yunsang Lee and Yongjun Lee for help with immunization of mice and fundoscopy, and Drs. Jian-Xin Lin, Yrina Rochman, and Rosanne Spolski, National Heart, Lung, and Blood Institute, for valuable discussions and critical comments. This work was supported by the Divisions of Intramural Research, National Heart, Lung, and Blood Institute and National Eye Institute and by the Basic Science Research Program through the National Research Foundation of Korea funded by the Ministry of Education, Science and Technology (Grant 2010-0010483 to H.-P.K.).

1. Spolski R, Leonard WJ (2008) Interleukin-21: Basic biology and implications for cancer and autoimmunity. *Annu Rev Immunol* 26:57–79.
2. Noguchi M, et al. (1993) Interleukin-2 receptor gamma chain mutation results in X-linked severe combined immunodeficiency in humans. *Cell* 73:147–157.
3. Leonard WJ (2001) Cytokines and immunodeficiency diseases. *Nat Rev Immunol* 1: 200–208.
4. Weaver CT, Hatton RD, Mangan PR, Harrington LE (2007) IL-17 family cytokines and the expanding diversity of effector T cell lineages. *Annu Rev Immunol* 25:821–852.
5. Spolski R, Leonard WJ (2010) IL-21 and T follicular helper cells. *Int Immunol* 22:7–12.
6. Harada M, et al. (2006) IL-21-induced Bepsilon cell apoptosis mediated by natural killer T cells suppresses IgE responses. *J Exp Med* 203:2929–2937.
7. Zeng R, et al. (2005) Synergy of IL-21 and IL-15 in regulating CD8+ T cell expansion and function. *J Exp Med* 201:139–148.
8. Kasaian MT, et al. (2002) IL-21 limits NK cell responses and promotes antigen-specific T cell activation: A mediator of the transition from innate to adaptive immunity. *Immunity* 16:559–569.
9. Ozaki K, et al. (2004) Regulation of B cell differentiation and plasma cell generation by IL-21, a novel inducer of Blimp-1 and Bcl-6. *J Immunol* 173:5361–5371.
10. Ozaki K, et al. (2002) A critical role for IL-21 in regulating immunoglobulin production. *Science* 298:1630–1634.
11. Brandt K, Bulfone-Paus S, Foster DC, Rückert R (2003) Interleukin-21 inhibits dendritic cell activation and maturation. *Blood* 102:4090–4098.
12. Spolski R, Kashyap M, Robinson C, Yu Z, Leonard WJ (2008) IL-21 signaling is critical for the development of type I diabetes in the NOD mouse. *Proc Natl Acad Sci USA* 105: 14028–14033.
13. Sutherland AP, et al. (2009) Interleukin-21 is required for the development of type 1 diabetes in NOD mice. *Diabetes* 58:1144–1155.
14. Bubier JA, et al. (2009) A critical role for IL-21 receptor signaling in the pathogenesis of systemic lupus erythematosus in BXSB-Yaa mice. *Proc Natl Acad Sci USA* 106: 1518–1523.
15. Herber D, et al. (2007) IL-21 has a pathogenic role in a lupus-prone mouse model and its blockade with IL-21R.Fc reduces disease progression. *J Immunol* 178:3822–3830.
16. Young DA, et al. (2007) Blockade of the interleukin-21/interleukin-21 receptor pathway ameliorates disease in animal models of rheumatoid arthritis. *Arthritis Rheum* 56:1152–1163.
17. Vollmer TL, et al. (2005) Differential effects of IL-21 during initiation and progression of autoimmunity against neuroantigen. *J Immunol* 174:2696–2701.
18. Coquet JM, Chakravarti S, Smyth MJ, Godfrey DI (2008) Cutting edge: IL-21 is not essential for Th17 differentiation or experimental autoimmune encephalomyelitis. *J Immunol* 180:7097–7101.
19. Parrish-Novak J, et al. (2000) Interleukin 21 and its receptor are involved in NK cell expansion and regulation of lymphocyte function. *Nature* 408:57–63.
20. Ozaki K, Kikly K, Michalovich D, Young PR, Leonard WJ (2000) Cloning of a type I cytokine receptor most related to the IL-2 receptor beta chain. *Proc Natl Acad Sci USA* 97:11439–11444.
21. Sadlack B, et al. (1995) Generalized autoimmune disease in interleukin-2-deficient mice is triggered by an uncontrolled activation and proliferation of CD4+ T cells. *Eur J Immunol* 25:3053–3059.
22. Kim HP, Imbert J, Leonard WJ (2006) Both integrated and differential regulation of components of the IL-2/IL-2 receptor system. *Cytokine Growth Factor Rev* 17:349–366.
23. Suzuki H, et al. (1995) Deregulated T cell activation and autoimmunity in mice lacking interleukin-2 receptor beta. *Science* 268:1472–1476.
24. Willerford DM, et al. (1995) Interleukin-2 receptor alpha chain regulates the size and content of the peripheral lymphoid compartment. *Immunity* 3:521–530.
25. Laurence A, et al. (2007) Interleukin-2 signaling via STAT5 constrains T helper 17 cell generation. *Immunity* 26:371–381.
26. Amadi-Obi A, et al. (2007) TH17 cells contribute to uveitis and scleritis and are expanded by IL-2 and inhibited by IL-27/STAT1. *Nat Med* 13:711–718.
27. Nussenblatt RB (1990) The natural history of uveitis. *Int Ophthalmol* 14:303–308.
28. Nussenblatt RB (1991) Proctor Lecture. Experimental autoimmune uveitis: Mechanisms of disease and clinical therapeutic indications. *Invest Ophthalmol Vis Sci* 32:3131–3141.
29. Chi W, et al. (2008) Upregulated IL-23 and IL-17 in Behçet patients with active uveitis. *Invest Ophthalmol Vis Sci* 49:3058–3064.
30. Liu X, Lee YS, Yu CR, Egwuagu CE (2008) Loss of STAT3 in CD4+ T cells prevents development of experimental autoimmune diseases. *J Immunol* 180:6070–6076.
31. Xu H, et al. (2008) A clinical grading system for retinal inflammation in the chronic model of experimental autoimmune uveoretinitis using digital fundus images. *Exp Eye Res* 87:319–326.
32. Chan CC, et al. (1990) Pathology of experimental autoimmune uveoretinitis in mice. *J Autoimmun* 3:247–255.
33. Rizzo LV, et al. (1994) Interleukin-2 treatment potentiates induction of oral tolerance in a murine model of autoimmunity. *J Clin Invest* 94:1668–1672.
34. Hinrichs CS, et al. (2008) IL-2 and IL-21 confer opposing differentiation programs to CD8+ T cells for adoptive immunotherapy. *Blood* 111:5326–5333.
35. Bhat P, Castañeda-Cervantes RA, Doctor PP, Foster CS (2009) Intravenous daclizumab for recalcitrant ocular inflammatory disease. *Graefes Arch Clin Exp Ophthalmol* 247: 687–692.
36. Sen HN (2009) High-dose daclizumab for the treatment of juvenile idiopathic arthritis-associated active anterior uveitis. *Am J Ophthalmol* 148:696–703.
37. Datta S, Costantino N, Court DL (2006) A set of recombineering plasmids for gram-negative bacteria. *Gene* 379:109–115.
38. Wang L, Jackson WC, Steinbach PA, Tsien RY (2004) Evolution of new nonantibody proteins via iterative somatic hypermutation. *Proc Natl Acad Sci USA* 101:16745–16749.